Environmental Science and Pollution Research (2024) 31:58335–58352
https://doi.org/10.1007/s11356-024-34992-2

RESEARCH ARTICLE

An insight into PANI-TiO_2 photocatalysis of refractory organic matter through molecular size fractionation

Ceyda Senem Uyguner-Demirel[1] · **Nazli Turkten**[2] · **Miray Bekbolet**[1]

Received: 14 February 2024 / Accepted: 11 September 2024 / Published online: 23 September 2024

Abstract

Refractory organic matter (RfOM) is ubiquitous in aquatic environment and plays various roles in regulating the fate, transport, toxicity, and bioavailability of chemical species, such as metals, emerging organic contaminants, and nanomaterials. RfOM is mainly represented by humic acids (HA) as the acid insoluble fraction of organic matrix. Considering the complex and multicomponent characteristic of HA, a detailed study was designed to elucidate the fate of molecular size fractions (MSFrs) of humic under solar irradiation in the presence of polyaniline (PANI)-modified TiO_2 composites. Humic acid as a consortium of diverse molecular size fractions with different tendencies towards oxidation requires further assessment by UV–vis and fluorescence spectroscopic parameters complementary to previous studies on the photocatalytic degradation of RfOM by using TiO_2 and PANI-TiO_2 composites. Absorbance-based removal efficiencies under initial and post-photocatalytic conditions showed a re-formation trend during photocatalysis in the presence of PANI and TiO_2 where higher MSFrs were transformed to lower MSFrs that was apparent for < 3 kDa fraction. Completely different profiles were observed for PT-41 and PT-81 indicating similar degradation pathways independent of PANI ratio in the composite. As confirmed by the investigated parameters, formation of both 450 kDa and 220 kDa MSFrs were evident under all conditions indicating in situ generation of higher MSFrs. The eligibility of coupled absorbance-fluorescence measurements to discern molecular size distribution of humic acid via oxidative degradation was also investigated. Excitation-emission matrix (EEM) contour plots emphasized the ratio dependency of PANI modification of TiO_2 and revealed sample specific variations that were more pronounced in terms of the emergence of tyrosine- and tryptophan-like aromatic proteins.

Keywords Molecular size fractions · PANI-TiO_2 · Solar photocatalysis · Refractory organic matter · UV–vis and fluorescence spectroscopic parameters

Introduction

The presence of dissolved organic matter (DOM) in nature holds prime importance from human health and environment point of view. In this respect, non-biodegradable refractory organic matter (RfOM) is omnipresent in aquatic environments and plays an important role in regulating the fate, transport, toxicity, bioavailability, and biogeochemical cycles of chemical species, including metals, emerging organic contaminants, even nano materials (Feng et al. 2022; Wang et al. 2022). Due to the heterogenous nature of organic matrix, in sun-lit waters, RfOM could express molecular size-dependent chemical and photo-chemical reactivity as well as a remediation role in bioavailability and toxicity (Li et al. 2023a). As the main component of DOM in aquatic systems, humic substances (HS) comprise the major carbon pool in the biosphere (1600×10^{15}gC). Depending on the solubility properties that are pH-controlled, HS are composed of three fractions as fulvic acids, humic acids (HAs), and humin. HAs are insoluble under acidic (pH < 3) conditions and are assemblies of a complex mixture of molecules of different size and structures in which chemical properties dynamically associate and stabilize by noncovalent interactions (Lipczynska-Kochany 2018). The ill-defined structural diversity is regarded as an anionic polyamphiphile expressed

Responsible Editor: Sami Rtimi

✉ Ceyda Senem Uyguner-Demirel
uygunerc@bogazici.edu.tr

[1] Institute of Environmental Sciences, Bogazici University, Bebek, Istanbul 34342, Türkiye

[2] Department of Chemistry, Faculty of Arts and Sciences, Kirsehir Ahi Evran University, Kirsehir, Türkiye

by molecular descriptors, i.e., aromaticity and aliphaticity derived from highly condensed hydrophobic backbones and hydrophilic side chains. HA is a consortium of molecular sub-fractions ranging in between 10^2 Da to 10^2 kDa, thus defined as highly heterogeneous and polydisperse in nature (Thurman et al. 1982; Xu and Guo 2017). Current research was directed to understanding of HAs as both macromolecules and supramolecular aggregates comprised smaller organic units of molecular weight < 1 kDa (Baigorri et al. 2007a, b; Schaumann 2006a, b). Supramolecular structures are mainly multimolecular in nature as held by hydrogen bonding, electrostatic and weak intermolecular interactions. Moreover, supramolecular structures are mainly affected by pH conditions of the aqueous medium, as well as by solar irradiation due to photosensitization effect of solar irradiation (Petrov et al. 2017).

Generally, HA was considered as a simple organic acid excluding polydispersity and heterogeneous nature; however, specific information on the structural diversity is limited (Ilina et al. 2014). The polydispersity of HA as molecular size could be verified by several techniques such as gel permeation chromatography and ultrafiltration, whereas freezing point depression method gives only number-averaged molecular weights. Ultrafiltration delineates humic molecular size distribution profiles as affected by configuration and charge of the sub-fractions. Molecular size variations in RfOM could strongly influence UV–vis absorption properties thereby the observed reactivities prevailing under aquatic systems. So far, the molecular size distribution of humic acids both in relation to natural origins and during treatment schemes has been studied extensively (Uyguner and Bekbolet 2005a, b). Bekbolet and colleagues investigated the effect of photocatalysis on humic molecular size fractions upon use of diverse photocatalysts (Uyguner-Demirel et al. 2022; Turkten and Bekbolet 2020).

Heterogeneous photocatalysis is widely considered as an alternative degradation process due to its non-selective oxidation mechanism and achievement of full mineralization. On the other hand, the main disadvantage of UVA-light dependency had also extended research efforts to testing various modifications of the photocatalysts as well as implementing photocatalytic degradation systems that are very well documented in literature (Li et al. 2023b; Constantino et al. 2022; Jiang et al. 2021; Etacheri et al. 2015). As a novel approach, the incorporation of a conducting polymer, polyaniline (PANI) was demonstrated to be advantageous in preparation of TiO_2 composites, i.e., PANI-TiO_2 (Turkten et al. 2021). In this respect, photocatalysis has been applied for the degradation of RfOM using solar light sensitive conducting polymer photocatalyst specimens (Uyguner-Demirel et al. 2023; Turkten et al. 2023).

Depending on the variations of PANI ratios in PANI-TiO_2 composites, photocatalysts expressed considerable performance for the removal of humic matter as a model compound of RfOM. PANI-TiO_2 and RfOM system displayed a plausible degradation mechanism based on both sensitization and synergy of counterparts upon solar irradiation. Humic matter was also considered as a compound responsible for catalyst deactivation during TiO_2 photocatalysis due to adsorptive interactions resulting in surface blockage and thereby diminished the number of active sites (Aguiar and Siqueira 2022). However, in-dept visualization of humic matter revealed that such a modeling approach would not explain the role of multi molecular size of humic fractions. Therefore, humic molecular size distribution patterns should be elucidated under photocatalytic conditions with specific interest on the type of photocatalyst used.

Photocatalytic treatment of various organic and inorganic substances as well as microbiological species have received wide attention since decades. Degradation of the parent substrates were often accompanied by investigation of the components of solution matrix even extending to toxicity of the products. However, in case of humic matter, degradation by-products would be actually "hidden humic sub-fractions" being transformed/reformed via non-selective oxidation mechanism. Consequently, assessment of the alterations in humic MSFrs by UV–vis and fluorescence spectroscopy would bring valuable information complementary to previous studies on the photocatalytic degradation of RfOM by using TiO_2 and PANI-TiO_2 composites (Turkten et al. 2023; Uyguner-Demirel et al. 2023). As described, humic acid should be considered as a consortium of diverse molecular size fractions each expressing different tendencies towards oxidation. Therefore, an in-dept study was designed to elucidate the fate of humic molecular size fractions under solar irradiation initiated photocatalysis. UV–vis spectroscopic parameters of humic fractions were characterized by specified absorbances, i.e., $Color_{436}$, UV_{365}, UV_{280}, and UV_{254}, followed by absorbance quotients, i.e., A_{254}/A_{436}, A_{254}/A_{365}, and A_{253}/A_{203}, as well as dissolved organic carbon (DOC) content normalized specific UV–vis parameters details of which were presented elsewhere (Uyguner and Bekbolet 2005a, b; Uyguner-Demirel et al. 2023). DOC normalized synchronous scan fluorescence parameters (FI_{syn}/DOC) and excitation-emission matrix (EEM) fluorescence patterns were also presented.

Methodology

Materials

Photocatalyst specimens: TiO_2 P-25 was supplied from Evonik. PANI and PANI-TiO_2 specimens were prepared according to procedure reported by Turkten and colleagues (Turkten et al. 2023). In PANI-TiO_2 composites, the selected

mole ratios of aniline/TiO_2 were 1:8, 1:4, 1:1, 4:1, and 8:1; hence, composites were denoted as PT-18, PT-14, PT-11, PT-41, and PT-81, respectively. Detailed information on the preparation methodology and physico-chemical properties of the photocatalyst specimens was presented in a previous study by Turkten and colleagues (Turkten et al. 2023).

Substrate: HA sodium salt as the model compound of RfOM was purchased from Aldrich (Sigma-Aldrich). A 1000 mg/L stock solution of HA was prepared in deionized/distilled water. Upon dilution to 50 mg/L HA solution, working solution RfOM as 100 kDa MSFr was obtained via ultrafiltration method by stirred cell ultrafiltration apparatus (Amicon 8050) with appropriate membrane filter cutoff.

Photocatalysis

Photocatalysis was performed using a Solar Simulator Atlas Suntest CPS + (Ref. 56,052,371) instrument equipped with an air-cooled Xenon lamp with emission wavelength range of 300–800 nm. Light intensity was determined by ferrioxalate actinometry as $I_o = 1.67$ µE/min (Hatchard and Parker 1956). Irradiation period of 60 min was selected to achieve detectable UV–vis and fluorescence spectroscopic parameters avoiding extensive degradation extents (Turkten et al. 2023; Uyguner-Demirel et al. 2023). The photocatalyst dose was kept constant as 0.25 mg/mL. The experiments were performed at room temperature (25 °C ± 2) under non-adjusted neutral pH conditions. The stirring speed of the magnetic stirrer was set to 320 rpm to avoid vortex formation in the slurry.

Ultrafiltration

Following photocatalysis, dual filtration through 0.45-µm and 0.22-µm membrane filters was applied. Samples were further subjected to fractionation by sequential stage ultrafiltration through membranes with nominal molecular weight cutoffs as 100 kDa, 30 kDa, 10 kDa, and 3 kDa. Operating pressures were 1 kg/cm^2 for 100-kDa, and 3 kg/cm^2 for 30-kDa, 10-kDa, and 3-kDa membrane filters. Separately collected filtrates were ascribed as 450 kDa, 220 kDa, 100 kDa, 30 kDa, 10 kDa, and 3 kDa MSFrs, respectively. All ultrafiltration membranes were thoroughly cleaned before use with 0.05 M NaOH solution, 0.02 M HCl, and ultrapure water, successively (Uyguner and Bekbolet 2005b).

RfOM descriptive parameters

UV–vis absorbance spectral profiles were acquired on A Perkin Elmer Lambda 35 spectrophotometer using 1-cm quartz cuvettes in wavelength range of 200–600 nm. Specified UV–vis parameters were selected absorbance recordings at specific wavelengths of 436 nm, 365 nm, 280 nm, and 254 nm and defined as $Color_{436}$, UV_{365}, UV_{280}, and UV_{254}, respectively. UV–vis absorbance quotients were absorbance ratios at selected wavelengths represented as A_{254}/A_{436}, A_{254}/A_{365}, and A_{253}/A_{203}. Specific UV absorbance ($m^{-1}L/mg$) defined as $SUVA_{254}$ or $SUVA_{280}$ was calculated by normalization of UV_{254} or UV_{280} to respective DOC (mg org C/L) content of humic solution. DOC contents were determined by A Shimadzu Vwp Total Organic Carbon analyzer in nonpurgeable organic carbon mode calibrated by using potassium phthalate (range 0–25 mg/L). A Perkin Elmer LS 55 Luminescence Spectrometer equipped with a 150 W xenon arc lamp and a red sensitive photomultiplier tube was used for the characterization of fluorescence features. Synchronous scan fluorescence spectra were acquired in the excitation wavelength range of 200–600 nm with $\Delta\lambda = 18$ nm between the excitation and emission monochromators. All synchronous scan fluorescence spectra were normalized to respective DOC contents (FI_{syn}/DOC) (Matthews et al. 1996; Peuravuori et al. 2002). Excitation-emission matrix (EEM) fluorescence spectra were recorded by simultaneous incremental changes in both excitation (λ_{exc}: 200 to 500 nm) and emission wavelengths (λ_{emis}: 200 to 600 nm). Three-dimensional EEM contour plots were derived from the data and modelled using MATLAB R2013a program. EEM fluorescence features were elucidated by five regions that were ascribed as Region I: Aromatic Proteins I, tyrosine-like (λ_{exc} 220–250 nm and λ_{emis} 280–332 nm), Region II: Aromatic Proteins II, tryptophan-like (λ_{exc} 220–250 nm and λ_{emis} 332–380 nm), Region III: Fulvic-like (λ_{exc} 220–250 nm and λ_{emis} 380–580 nm), Region IV: Microbial byproducts (λ_{exc} 250–470 nm and λ_{emis} 280–380 nm), and Region V: Humic-like (λ_{exc} 250–470 nm and λ_{emis} 380–580 nm) (Sen-Kavurmaci and Bekbolet 2014). For clarity purposes, a pictorial presentation of regional distribution of EEM fluorescence contour plots is illustrated in Supplementary Information part (Fig. S1).

Results and discussion

Molecular size distribution of RfOM following photocatalysis

Humic matter generally displays a wavelength-dependent, broad, and featureless spectrum as a consequence of underlying complex intramolecular cumulative interactions of various chromophores and fluorophores in its structure. Therefore, numerous UV–vis absorbance and fluorescence parameters were extensively used in elucidation of conformational as well as configurational variations in relation to molecular size fractions (Chen and Yu 2021; Trubetskoj et al. 2018; Uyguner and Bekbolet 2005a, b; Uyguner-Demirel and Bekbolet 2011).

Upon photocatalysis, UV–vis-specified parameters revealed the presence of higher MSFrs, i.e., 450 kDa and 220 kDa that could be explained by aggregation of lower molecular size fractions via weak interactions such as van der Waals, $\pi - \pi$, and CH-π as well as intra- or inter-molecular interactions (Ni and Pignatello 2018; Šmejkalová and Piccolo 2008). Moreover, enhanced absorption in UV region could also be related to changes in the structure and/or contents of chromophores, e.g., –OH, benzene rings substituted with –COOH, intramolecular electron donor acceptor complexes, and other complex unsaturated conjugated chromophores (Qi et al. 2004).

UV–vis spectroscopic properties

During the course of photocatalysis, MSFrs of RfOM were exposed to diverse degradation patterns. Since each MSFr was composed of similar overlapping structural units, the outcome could be expressed by the simultaneous removal of chromophores reflected as a decrease of absorbance or re-formation of chromophores indicating an increase of absorbance that would consequently effect UV–vis parameters.

Removal/Re-formation efficiencies (%) were calculated as follows:

$$\text{Removal/Re} - \text{formation efficiency} = [(\text{Abs}_o - \text{Abs}_f)/\text{Abs}_o] \times 100$$

where Abs_o and Abs_f denoted selected UV–vis parameters (Color_{436}, UV_{365}, UV_{280}, and UV_{254}) under initial and post-photocatalytic conditions.

Basically, removal efficiency would be presented as a positive number since Abs_o would be greater than Abs_f, whereas re-formation efficiency could be represented by a negative number since Abs_f would be greater than Abs_o. Figure 1A–G was designed to emphasize the differences in removal and re-formation efficiencies of MSFrs.

PANI was shown to act as a p-type photocatalyst due to its high reducing potential and low band energy (Ekande and Kumar 2021). In the presence of bare PANI, MSFrs > 10 kDa were concomitantly removed by surface adsorption as well as by photocatalysis. The lowest MSFr as 3 kDa expressed a re-formation trend during photocatalysis where higher MSFrs were transformed to lower MSFrs. Moreover, this re-formation trend indicating enhanced absorption in the UV region may also be related to changes in the structure and/or contents of chromophores (Qi et al. 2004). PANI displayed amphiphilic nature due to the presence of hydrophobic benzenoid and quinoid parts while the amine and imine groups could form hydrogen bonds with water molecules. The surfactant properties of both counterparts, i.e., PANI and MSFrs of RfOM could possibly interact with each other thereby facilitate adsorptive interactions. Since RfOM and PANI binary solution was filtered through 0.45 μm membrane filter prior to the application of sequential ultrafiltration, discrimination between these processes could not be verified. PANI was shown to be highly susceptible to humic adsorption; however, since then, no interest was devoted to undermine the molecular size effects (Li et al. 2011; Wang et al. 2012; Zhang et al. 2010). During photocatalysis, PANI could provide extended surface area affecting the resultant conformational arrangements, thereby, altering the molecular size fractionation patterns of RfOM. PANI amount would be directly effective on formation of multiple conformations of different molecular size fractions composed of both non-degraded-native and oxidized-degraded organic moieties (Li et al. 2021). On the other hand, persistent free radical formation potentials revealed that low molecular weight fractions (MWF, < 3500, < 7000, and < 14,000 Da) could be assigned to oxygen-centered organic radicals while high MWF (> 14,000 Da) were assigned to carbon-centered organic radicals that were also related to formation of reactive oxygen species (ROS) (Shi et al. 2021; Uyguner-Demirel et al. 2023).

Upon TiO_2 photocatalysis, removal efficiency pattern displayed a molecular size dependent decreasing profile except for 3 kDa MSFr (Uyguner-Demirel et al. 2022). Formation efficiency of lower molecular size fractions (< 3 kDa) was more pronounced for UV absorbing centers (UV_{254} and UV_{280}) in comparison to color forming moieties (Color_{436}). UV absorbing groups were related to dense aromatic and carboxylic electron centers rich in π-electron systems (e.g., phenolic arenes, benzoic acids, and polycyclic aromatic structures) whereas Color_{436} represented keto-enol systems and quinoid structures revealing absorption in the visible light region (Bekbolet and Kavurmaci 2015; Uyguner and Bekbolet 2005b). The adsorption of in situ oxidized HA was considered as the main reason forming surface complexes with TiO_2, blocking the active sites of the photocatalyst and eventually decreasing the efficiency of photogenerated charge transfer during long adsorption process (Yang et al. 2021).

Incorporation of PANI into TiO_2 diverted the mechanism of photocatalysis/photocatalytic behavior from both PANI and TiO_2 (Fig. 1A, B). Upon use of PT-11 (Fig. 1C), a distinct discrimination was evident between color forming centers and UV absorbing centers for all MSFrs except for fractions less than 3 kDa. Re-formation of color forming (Color_{436}) and UV absorbing (UV_{365}) groups was more pronounced for all MSFrs along with successive removal of UV_{254} and UV_{280}. On the other hand, < 3 kDa fraction displayed re-formation of lower molecular size fraction upon transformation of all molecular size fractions. The effect of increasing PANI content in the composites, i.e., PT-41 and PT-81, resulted in removal of all UV–vis parameters (~ 60–70%) of MSFrs in an almost similar fashion from 450 to 10 kDa fractions

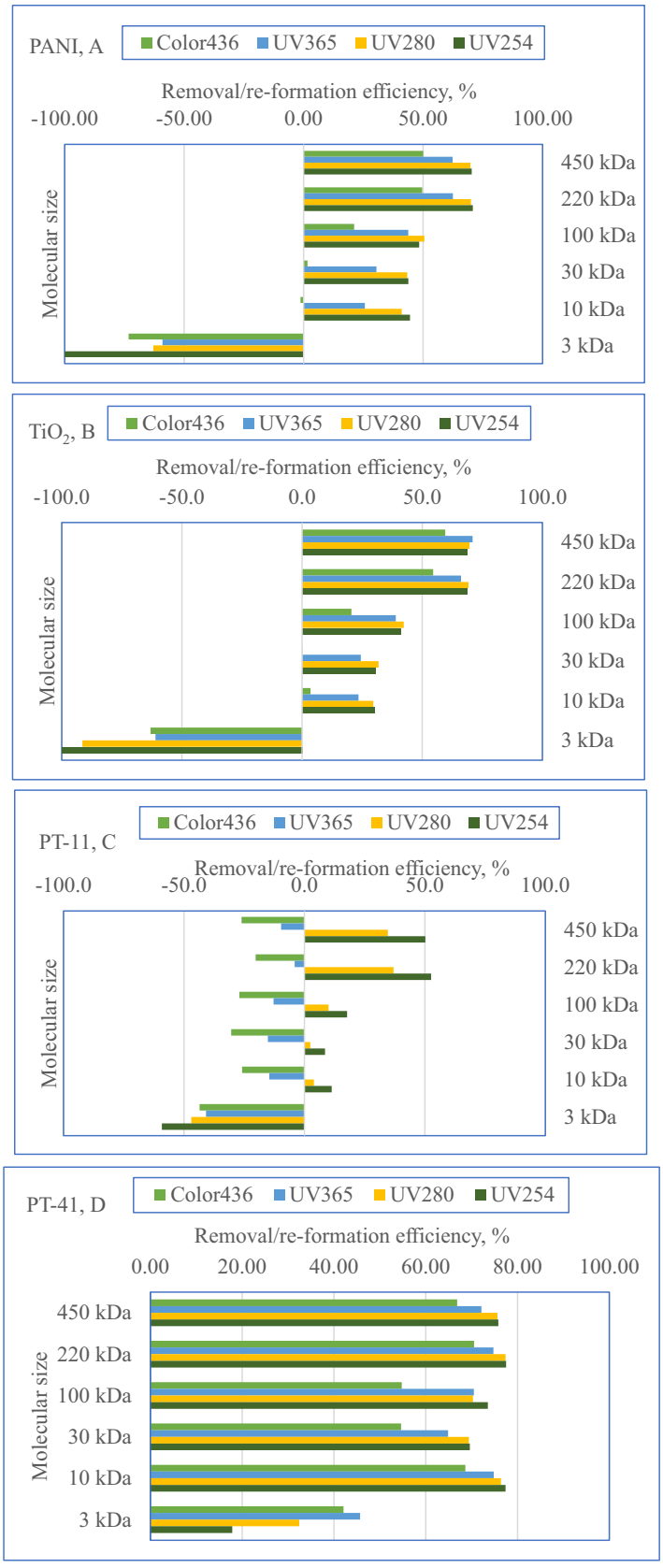

Fig. 1 **A**–**G** Removal/re-formation efficiency pattern of the specified UV–vis parameters of MSFrs of RfOM upon photocatalysis using PANI (A), TiO_2 (B), PT-11 (C), PT-41 (D), PT-81 (E), PT-14 (F), and PT-18 (G)

Fig. 1 (continued)

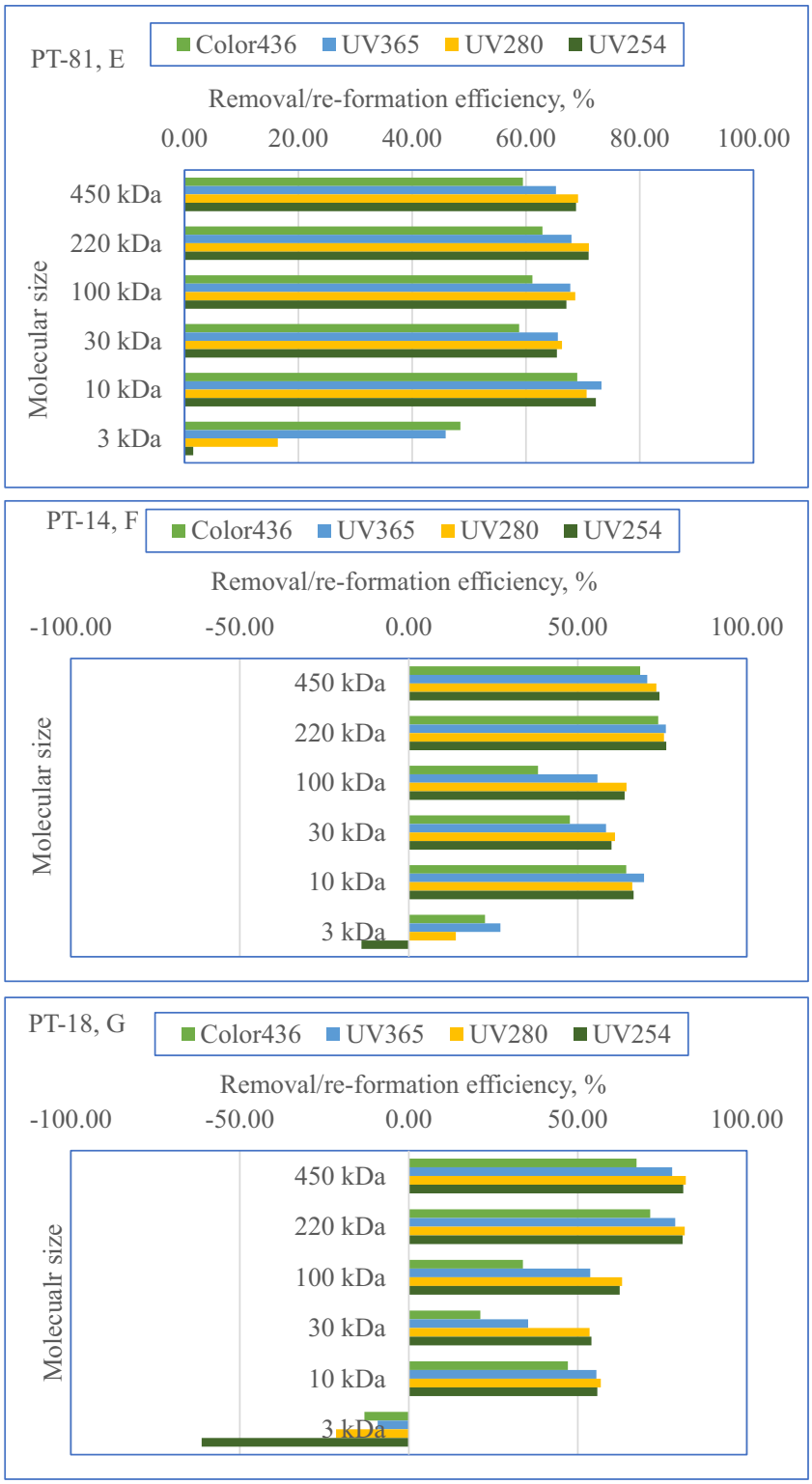

(Fig. 1D, E). Noteworthy similarity in respective removal of molecular size fractions for both PT-41 and PT-81 might indicate similar degradation pathway independent of PANI ratio in the composite. The most significant effect was observed for < 3 kDa fraction in a decreasing order of $Color_{436} > UV_{365} > UV_{280} > > > UV_{254}$ (1.5%). This phenomenon could be related to the adsorptive interactions dominating over photocatalysis upon irradiation. The role of filtration through 0.45-μm membrane filter should be encountered as the primary step of selective

removal prior to sequential ultrafiltration. It should also be noted that degradation kinetics of all UV–vis parameters revealed rate constants that were relatively lower for PT-41 and PT-81 in comparison to other composites (Uyguner-Demirel et al. 2023). Increasing TiO_2 content of composites as PT-14 and PT-18 reflected almost similar tendencies to PT-41 and PT-81 with some discrepancies (Fig. 1F, G). The role of adsorption due to the presence of PANI would be suppressed by the extended light absorption capacity of TiO_2 that would result in degradation of humic units irrespective of the molecular size. From this point of view, the diversity in molecular size fractionation profiles would mostly be related to prevailing non-selective oxidation pathways. More significantly, a direct comparison of the profiles of PT-41 and PT-81 could possibly reveal the effect of the composite properties on lower MSFrs as < 3 kDa in a progressive manner.

Previous studies revealed the effect of PANI incorporation into TiO_2 upon solar photocatalysis using RfOM as a substrate (Turkten et al. 2023; Uyguner-Demirel et al. 2023). Degradation of RfOM was followed by a gross parameter as DOC along with UV–vis and fluorescence spectroscopic features. Uyguner and colleagues reported that the synergetic effect between PANI and TiO_2 was more pronounced in lower PANI ratios, whereas higher PANI ratios reflected a retardation effect up to a specific mass ratio of polyaniline to TiO_2 (Uyguner-Demirel et al. 2023). Considering that RfOM mainly consisted of diverse molecular size fractions each operating as single organic entities, the resultant effect could well be displayed by removal of higher MSFrs and re-formation of lower MSFrs via both transformation and self-removal pathways irrespective of the photocatalyts type.

Based on this information, presence of RfOM molecular size fractions as well as adsorbed RfOM-PANI onto TiO_2 could lead to conditions that could be considered as effective on degradation efficiencies. Due to effective p–n junction of the composites along with the photosensitizing properties of both PANI and RfOM, oxidative and reductive pathways could prevail resulting in variations in removal/re-formation efficiencies.

UV–vis spectroscopic quotients

An in-depth understanding of UV–vis absorbance spectra is mainly based on the ratios of the absorbance values measured at selected wavelengths to quantify the physiochemical characteristics of the interactions of MSFrs upon photocatalysis. Monotonously declining UV–vis spectral features could bring more specific information upon use of absorbance ratios defined as A_{254}/A_{436}, A_{254}/A_{365}, and A_{253}/A_{203} quotients. From a general perspective, each photocatalyst specimen displayed the following decreasing order of the selected absorbance quotients:

A_{254}/A_{436}:

PANI : 100 kDa > 450 kDa > 220 kDa > 30 kDa > 10 kDa > 3 kDa
TiO2 : 450 kDa > 100 kDa > 10 kDa > 3 kDa > 30 kDa > 220 kDa
PT – 11 : 220 kDa > 450 kDa > 100 kDa > 3 kDa ~ 30 kDa > 10 kDa
PT – 41 : 220 kDa > 450 kDa > 10 kDa > 30 kDa > 3 kDa > 100 kDa
PT – 81 : 10 kDa > 3 kDa > 100 kDa > 30 kDa > 220 kDa > 450 kDa
PT – 14 : 10 kDa > 220 kDa > 450 kDa > 30 kDa > 3 kDa > 100 kDa
PT – 18 : 10 kDa > 220 kDa > 3 kDa > 100 kDa > 450 kDa > 30 kDa

A_{254}/A_{365}:

PANI : 100 kDa > 30 kDa > 220 kDa > 450 kDa > 10 kDa ~ 3 kDa
TiO2 : 450 kDa > 100 kDa > 220 kDa > 10 kDa > 3 kDa > 30 kDa
PT – 11 : 30 kDa > 220 kDa > 3 kDa > 100 kDa > 10 kDa > 450 kDa
PT – 41 : 10 kDa > 100 kDa > 3 kDa > 220 kDa > 30 kDa > 450 kDa
PT – 81 : 3 kDa > 10 kDa > 100 kDa > 30 kDa > 220 kDa > 450 kDa
PT – 14 : 10 kDa > 220 kDa > 30 kDa > 3 kDa > 450 kDa > 100 kDa
PT – 18 : 10 kDa > 220 kDa > 3 kDa > 450 kDa > 100 kDa > 30 kDa

A_{253}/A_{203}:

PANI : 450 kDa > 220 kDa > 10 kDa > 3 kDa > 30 kDa > 100 kDa
TiO2 : 30 kDa > 3 kDa > 10 kDa > 220 kDa > 450 kDa > 100 kDa
PT – 11 : 450 kDa > 220 kDa > 100 kDa > 10 kDa > 30 kDa > 3 kDa
PT – 41 : 450 kDa > 220 kDa > 30 kDa > 10 kDa > 3 kDa > 100 kDa
PT – 81 : 450 kDa > 220 kDa > 100 kDa > 10 kDa > 30 kDa > 3 kDa
PT – 14 : 450 kDa > 220 kDa > 100 kDa > 10 kDa > 30 kDa > 3 kDa
PT – 18 : 3 kDa > 100 kDa > 450 kDa > 10 kDa > 220 kDa > 30 kDa

A_{254}/A_{436} quotient signified the relative change of UV-absorbing centers with respect to color forming groups that are mostly composed of a heterogeneous mixture of aromatic and aliphatic fractions containing oxygen, nitrogen, and sulfur functional groups (e.g., phenolics, carbohydrates, amino groups, and furfurals) (Chen et al. 2003; Uyguner et al. 2007). On the other hand, UV-absorbing centers are related to structural units mainly composed of aromatic rings and used a proxy of aromaticity as well as DOC. Hence, the quotient could also bring information on the degradation of the phenolic/quinoid core of humic matter to simpler carboxylic aromatic compounds. The increase of A_{254}/A_{436} quotient for certain molecular size fractions could denote degradation of long-wavelength absorbing chromophores, including quinoid and semiquinoid arrangements, aromatic and/or heterocyclic zwitterions (e.g., aminochromes), and charge-transfer complexes (Michalska et al. 2023). However, observed trends were completely different upon use of different photocatalysts (Fig. 2). All samples exhibited lower values than the initial A_{254}/A_{436} quotient value of 6.258 expressing simultaneous removal of all centers/groups. A_{254}/A_{436} quotients of 450 kDa fractions were clustered upon photocatalysis excluding PANI and PT-18 specimens which strongly

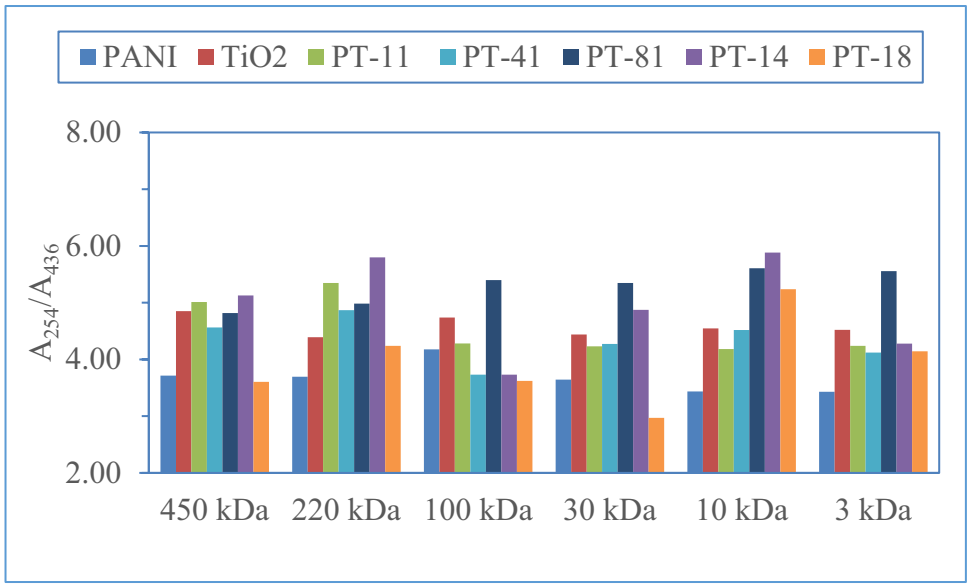

Fig. 2 Comparative presentation of A_{254}/A_{436} quotient of RfOM upon photocatalysis using PANI, TiO_2, PT-11, PT-41, PT-81, PT-14, and PT-18, respectively

indicated comparatively fast removal of the specified parameters. The lowest A_{254}/A_{436} quotient was attained for 30 kDa MSFr upon use of PT-18 composite. The reason could be attributed to surface properties of PT-18 for preferential degradation of 30 kDa MSFr. On the other hand, upon PT-14 photocatalysis, 10 kDa MSFr expressed comparatively higher A_{254}/A_{436} quotient indicating re-formation of the respective groups via oxidative/reductive mechanism.

A_{250}/A_{365} (designated as E_2/E_3 in reference publications) quotient was demonstrated to be a useful tool to follow the size changes in natural organic matter (De Haan and De Boer 1987; Peuravuori and Pihlaja 1997). Likewise, an increase in A_{254}/A_{365} quotient was reported to indicate a decrease in average molecular weight and aromaticity of humic substances upon irradiation (Dahlén et al. 1996). The molecular weight dependence of A_{254}/A_{365} quotient could be derived from an increased probability of electronic interactions between respective light absorbing centers in larger MSFrs. An inverse relationship was expected due to the stronger light absorption capacity of high MSFrs. However, upon solar irradiation, molecular weight and A_{254}/A_{365} relationship was demonstrated to follow a quasi-exponential function indicating that the quotient could well be regarded as a proxy of molecular weight estimation (Lou and Xie 2006). A_{254}/A_{365} quotient was correlated with quantum yields of $^1O_2$ and CO photoproduction, the mechanism of which could also be expected to be effective during photocatalysis of RfOM MSFrs exposed to solar irradiation (Dalrymple et al. 2010). Free, non-reacted RfOM sub-fractions present in aqueous medium could also undergo direct photoreactions leading to formation of lower MSFrs.

A_{254}/A_{365} quotients of all MSFrs were distinctly different from each other irrespective of the type of the photocatalyst specimen (Fig. 3). The lowest value was attained for 30 kDa fraction upon use of PT-18 composite while the highest was attained for 10 kDa MSFr upon use of PT-14 specimen. The reason could be attributed to the role of TiO_2 ratio in the composites leading to better photocatalytic performance which could be expressed by the selected quotient.

As specific UV parameters, $SUVA_{254}$ as well as $SUVA_{280}$ were associated with the levels of double bonds, chromophoric groups and molecular size of humic sub-units were thereby used as a proxy for aromaticity (Weishaar et al. 2003; Valencia et al. 2013). Since A_{254}/A_{365} quotient was also regarded as an indicative parameter of aromaticity, a correlative approach was investigated between A_{254}/A_{365} quotient and $SUVA_{280}$ parameter. All MSFrs expressed comparatively higher $SUVA_{280}$ (> 6) indicating the dominance of aromatic character under all conditions (Supplementary Materials, Fig. S2-S8). A 100-kDa fraction of RfOM exhibited the lowest aromaticity ($SUVA_{280}$) followed by a steady increase in lower molecular size fractions reaching almost the same initial $SUVA_{280}$. Contrary to this trend, as molecular size decreased, almost no change in A_{254}/A_{365} was observed except for a 100-kDa fraction. Therefore, no distinct correlation could be visualized between proxies of aromaticity and molecular size of organic fractions upon use of bare PANI under solar irradiation. Due to the presence of amine and imine groups in PANI, the surface charge of the molecule would be positive in the pH range of 2–10 and attract anionic substrates, e.g., polyphenolic pollutants as well as humic matter via adsorptive interactions (Wang et al. 2012, 2013; Goh et al. 2022). Hence, under solar radiation, PANI would definitely be facilitating adsorptive removal of humic fractions along with removal via photo-initiated reactions (Uyguner-Demirel et al. 2023).

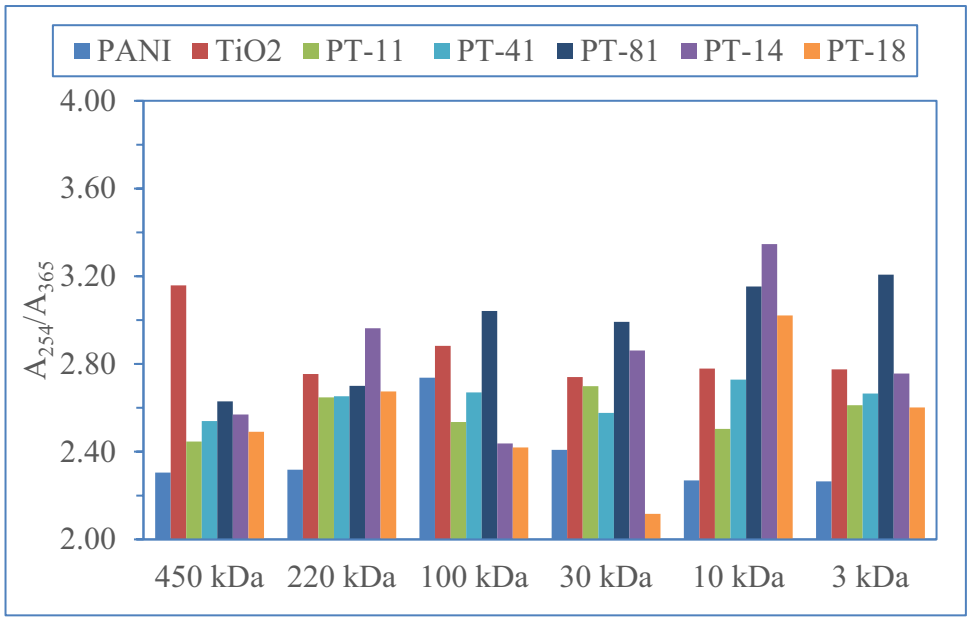

Fig. 3 Comparative presentation of A_{254}/A_{365} quotient of RfOM upon photocatalysis using PANI, TiO_2, PT-11, PT-41, PT-81, PT-14, and PT-18, respectively

Upon TiO_2 photocatalysis, 450 kDa MSFr expressed highest A_{254}/A_{365} quotient, whereas $SUVA_{280}$ remained almost constant irrespective of the molecular size. The reason could be attributed to the concomitant removal of UV_{280} absorbing aromatic centers (related to n-p* and p-p* transitions) along with DOC during TiO_2 photocatalysis (Uyguner-Demirel and Bekbolet 2011). Moreover, minor fluctuations of A_{254}/A_{365} could be related to the concurrent removal and re-formation of chromophores expressing absorbance in respective UV–vis region. Lower molecular weight fractions (< 30 kDa) displayed almost similar reactivity towards ROS attack resulting in removal of all UV–vis light sensitive region.

Upon use of PT-11, the role of PANI modification could be visualized through fluctuations in A_{254}/A_{365} quotients. In general, $SUVA_{280}$ being comparatively higher (~ 8) displayed the tendency of sole PANI photocatalysis. The most remarkable effect was observed in 100 kDa fraction being highly susceptible to degradation of UV_{280} absorbing centers contrary to the variations in A_{254}/A_{365} quotient revealing the role of longer wavelength absorbing chromophoric centers. Increasing PANI percentage in PT composite as PT-41 resulted in a steady increase in both aromaticity proxies for higher molecular size fractions up to 100 kDa fraction. A steady decrease of $SUVA_{280}$ was attained for 30 kDa and 10 kDa fractions followed by a slight increase in 3 kDa fraction. A_{254}/A_{365} displayed a similar pattern except for lower molecular size fractions < 30 kDa MSFr expressing the plausible role of surface characteristics due to the presence of PANI contributing to diverse interactions (Turkten et al. 2023). Further increase in PANI percentage in PT composite as PT-81 expressed a consistently increasing trend of A_{254}/A_{365} quotient for all molecular size fractions contrary to the observed tendency of $SUVA_{280}$. The effect of PANI could be visualized as dominating over TiO_2 during photocatalysis (Uyguner-Demirel et al. 2023). Both parameters expressed opposite trends for higher MSFrs that could be related to in situ formation of 450 kDa and 220 kDa fractions. This also confirmed the comparatively lower rate constants reported upon use of PT-81composite (Uyguner-Demirel et al. 2023).

Increasing TiO_2 percentage in PT composite as PT-14 resulted in a steady increase in both aromaticity proxies for higher MSFrs (> 100 kDa) followed by a steady decreasing trend in $SUVA_{280}$. A_{254}/A_{365} quotient displayed a diverse pattern with respect to decreasing molecular size. Further increase in TiO_2 percentage in PT composite as PT-18 expressed a completely inconsistent trend revealing insignificant correlation with molecular size.

A_{253}/A_{203} quotient was also introduced as a useful tool for monitoring changes in humic matter upon various conditions (Fig. 4). The absorption band at $\lambda = 253$ nm was related to the electron-transfer band in aromatic dense centers, whereas absorption band at $\lambda = 203$ nm signified the benzenoid bands due to vibrational perturbations in π-electron system. Concomitantly, A_{253}/A_{203} quotient was described as an indicator of unsaturated /saturated fraction proportions in organic matrix related to the abundance of substituted functional groups linked to aromatic structures (Korshin et al. 1997; Li et al. 2023a). Comparatively higher ratios are related to the aromatic rings that contain carbonyl, carboxyl, hydroxyl, and ester groups, whereas lower ratios are related to the aliphatic chains. Typical values of A_{253}/A_{203} quotients were reported in between 0.25 and 0.35, whereas higher values above 0.40 indicated the presence of aromatic rings substituted

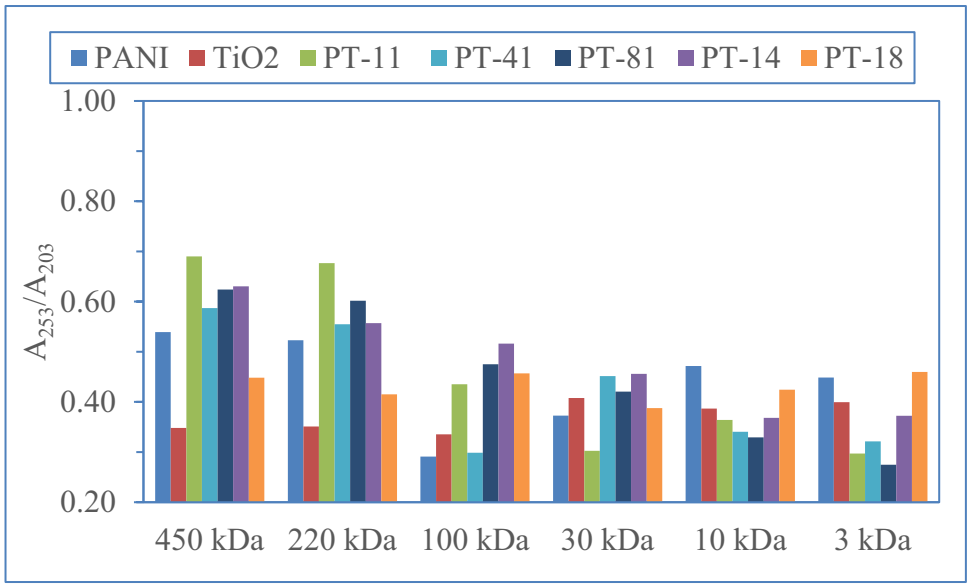

Fig. 4 Comparative presentation of A_{253}/A_{203} quotient of RfOM upon photocatalysis using PANI, TiO_2, PT-11, PT-41, PT-81, PT-14, and PT-18, respectively

with carbonyl, carboxyl, and (especially) ester carboxylic groups (Scott 1964). Li and colleagues reported an inverse relationship between molecular size fractions and A_{253}/A_{203} quotients of Aldrich humic acid (Li et al. 2023a). This result was also in good agreement with size distribution and bulk 253 nm/203 nm absorbance ratio data of humic acid adsorption on quartz sand, which showed the initial adsorption of low molecular weight aromatic moieties (Pitois et al. 2008). Uyguner-Demirel and colleagues reported a decreasing profile of A_{253}/A_{203} quotient with decreasing MSFrs for HA and upon solar photolysis being more pronounced for lower MSFr (10 kDa) as well as upon Cu-doped TiO_2 photocatalysis (Uyguner-Demirel et al. 2022).

RfOM as represented by HA exhibited an initial A_{253}/A_{203} quotient as 0.765. From a general perspective, all MSFrs followed a decreasing profile irrespective of the photocatalyst specimen. The variations between quotients of A_{253}/A_{203} (0.35 to 0.70) were more evident for higher, i.e., 450 kDa and 220 kDa MSFrs expressing the role of re-formation via weak interactive forces (Šmejkalová and Piccolo 2008). Upon use of PANI or TiO_2 specimen, 100 kDa MSFr displayed considerably a lower value of A_{253}/A_{203} indicating the plausible formation of aliphatic groups. PT-11 specimen exerted a more pronounced effect on the structural changes as expressed by A_{253}/A_{203} quotient (<0.30) for the lower MSFrs (<30 kDa). Lower MSFrs <30 kDa exhibited quotients in the range of 0.28–0.48 expressing the formation of hydroxylated groups. The role of PANI modification of TiO_2 could not be visualized as exerting a consistent trend of A_{253}/A_{203} quotient with respect to the decreasing profile of MSFr. Therefore, direct assessment of humic composition with respect to A_{253}/A_{203} quotient would be inadequate. It should also be mentioned that the quotient A_{253}/A_{203} was independent of the resulting DOC contents upon use of the selected photocatalyst specimens (Uyguner-Demirel et al. 2023).

Fluorescence spectroscopic properties

Synchronous scan fluorescence properties

The completion of UV–vis spectrophotometric analyses of HS with an evaluation of fluorescence properties can provide broad information related to structure, conformation, and heterogeneity of organic matrix in relation to dynamic properties as a result of prevailing intramolecular and intermolecular interactions. Synchronous scan fluorescence spectra of humic matter exhibited a principal absorption near $\lambda_{emis} \sim 475$ to 480 nm (Miano et al. 1988; Uyguner and Bekbolet 2005b). In general, low molecular weight humic fractions expressed considerably higher fluorescence intensities than those of high molecular weight fractions. Higher fluorescence intensities at longer wavelengths were associated with the presence of carbonyl-containing substituents, hydroxyl, alkoxyl, and amino groups. Furthermore, humic sub-fractions that exhibited fluorescence at longer wavelengths with low intensity could be the linearly condensed aromatic rings and other unsaturated bond systems capable of a high degree of conjugation (Richard et al. 2011; Peuravuori et al. 2002).

DOC normalized synchronous scan fluorescence spectral features of RfOM MSFrs under post-photocatalytic conditions are illustrated in Fig. 5A–G. In general, differences in FI_{syn}/DOC patterns of all MSFrs indicated non-selective mechanism of photocatalysis leading to the formation of fluorophores in shorter emission wavelengths excluding the region $\lambda_{emis} > 400$ nm. Fluorescence spectral features of all MSFrs expressed a hypsochromic (blue)

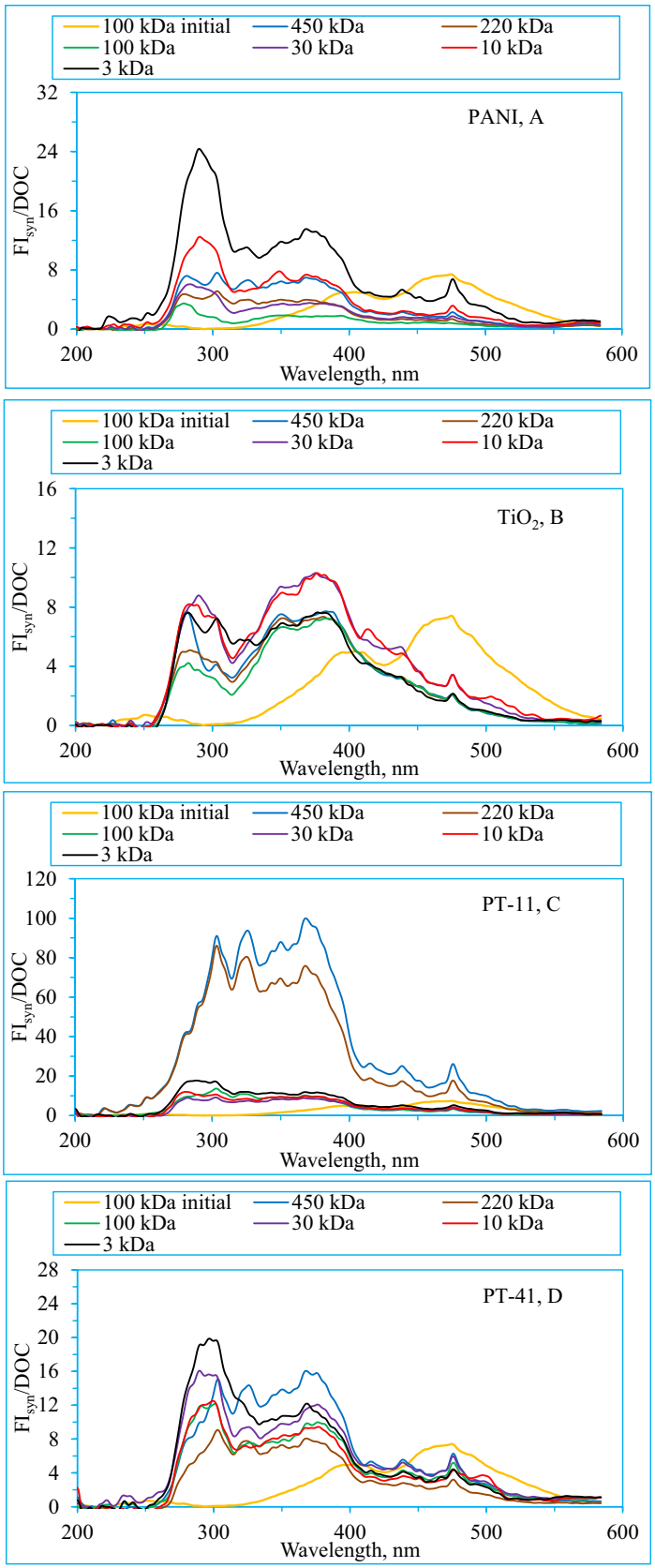

Fig. 5 **A**–**G** DOC normalized synchronous scan fluorescence spectral features (FI_{syn}) of MSFrs of RfOM under post-photocatalytic conditions upon use of PANI (A), TiO_2 (B), PT-11 (C), PT-41 (D), PT-81 (E), PT-14 (F), and PT-18 (G)

Fig. 5 (continued)

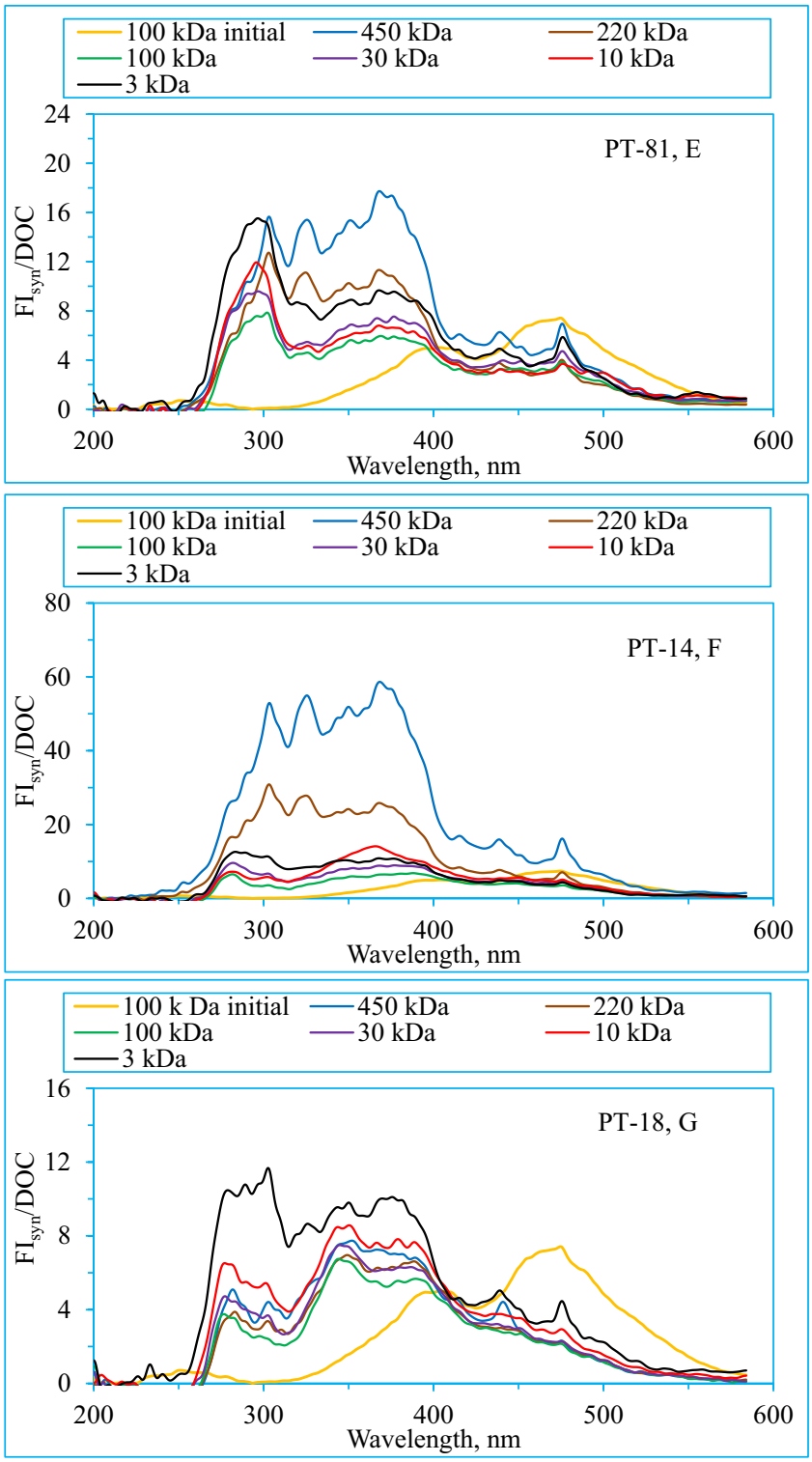

shift with intensities in reverse order of the molecular size. Initial 100 kDa MSFr of RfOM expressed a major peak around λ_{emis} ~ 475 nm with a shoulder around λ_{emis} > 400 nm as previously reported by Uyguner and Bekbolet (Uyguner and Bekbolet 2005b).

Direct exposure of RfOM to solar irradiation in the presence of sole PANI reflected a hypsochromic shift expressing a considerably higher FI_{syn} of 3 kDa MSFr in 250 nm < λ_{emis} < 400 nm. In this region, FI_{syn}/DOC of MSFrs followed a decreasing order as 3 kDa > 10 kDa > 30 kDa > 100 kDa

MSFr. The fluorophoric region around λ_{emis} ~ 350–400 nm was associated with highly conjugated aliphatic structures and polycyclic aromatics with three to four fused benzene rings. Moreover, fluorescence emission at longer wavelengths were ascribed to polycyclic aromatic structures with highly fused benzene rings.

TiO_2 photocatalysis revealed a remarkable shift of fluorophores to λ_{emis} < 400 nm expressing two major peaks at λ_{emis} ~ 280 nm and a broader peak at λ_{emis} < 380 nm irrespective of the molecular size. The formation of lower molecular size fractions through degradation of RFOM was evident as supported by UV–vis absorbance spectral features (Fig. 1). The fluorescence fingerprints of 450 kDa and 200 kDa MSFrs could be ascribed to the operational formation of higher molecular size fractions > 100 kDa. Following photocatalytic treatment using PT-11, the synchronous scan fluorescence spectral features of RfOM displayed a more pronounced, fraction-dependent variation especially for 450 kDa and 220 kDa expressing aggregation behavior (Baigorri et al. 2007a, b). High intensities could also be explained by unresolved overlapping behavior of fluorophores. However, all lower MSFrs were distinguished by their low fluorescence intensities. Upon PT-41 photocatalysis, all MSFrs expressed distinctly different FI_{syn}/DOC profiles as discriminated by a broad emission area in the wavelength region of λ_{emis} 275–400 nm. The highest FI_{syn}/DOC was attained for 3 kDa MSFr expressing the presence of dense fluorophoric groups at λ_{emis} ~ 300 nm. However, 450 kDa MSFr of RfOM displayed a broader fluorophoric region being centered at λ_{emis} ~ 400 nm. Upon use of PT-81 composite, a comparable profile to PT-41 was observed with relatively lower FI_{syn}/DOC of 3 kDa MSFr at λ_{emis} ~ 300 nm. Moreover, 450 kDa MSFr of RfOM displayed a broader fluorophoric region being centered at λ_{emis} ~ 400 nm. Following photocatalytic treatment using PT-14, synchronous scan fluorescence spectral features of RfOM displayed molecular size fraction dependent variations especially for 450 kDa and 200 kDa MSFrs expressing aggregation behavior as was attained for PT-11 photocatalysis. Upon photocatalysis, in the presence of PT-18 representing higher TiO_2 content, almost all fluorophores were completely removed except 3 kDa MSFr exhibiting FI_{syn}/DOC ~ 12 in 250 nm < λ_{emis} < 400 nm region (Fig. 5A–G).

EEM fluorescence features

EEM fluorescence contour plots were evaluated using a similar technique as described previously by Sen-Kavurmacı and Bekbolet (Kavurmaci and Bekbolet 2014). EEM contour plots are given in Supplementary Materials (Figs. S9–S16), and data compiled from regional speciation of EEM fluorescence spectral features are presented in Table 1. The strength of fluorescence intensity was indicated by a symbol (+) with reference to the presented color intensity. EEM fluorescence features were elucidated by five regions that were ascribed as:

Region I: Aromatic Proteins I, tyrosine-like (λ_{exc} 220–250 nm and λ_{emis} 280–332 nm).
Region II: Aromatic Proteins II, tryptophan-like (λ_{exc} 220–250 nm and λ_{emis} 332–380 nm).
Region III: Fulvic-like (λ_{exc} 220–250 nm and λ_{emis} 380–580 nm).
Region IV: Microbial by-products (λ_{exc} 250–470 nm and λ_{emis} 280–380 nm).
Region V: Humic-like (λ_{exc} 250–470 nm and λ_{emis} 380–580 nm).

PANI:

Region II dominated over Region I expressing the presence of both tyrosine-like and tryptophan-like aromatic proteins especially for higher MSFrs (> 10 kDa). The presence of fulvic-like fluorophoric groups (Region III) were evident for all MSFrs being more pronounced for lower MSFrs (< 10 kDa). Region IV could only be visualized for 10 kDa and 3 kDa MSFrs. Lower MSFrs displayed more humic-like fluorophoric region in comparison to higher MSFrs (> 30 kDa MSFr).

TiO_2:

Both Region I (except 30 kDa MSFr) and Region II were evident for all MSFrs indicating the contribution of both tyrosine-like and tryptophan-like aromatic proteins. The presence of fulvic-like fluorophoric groups were more pronounced than humic-like fluorophores. Minor peaks indicate the presence of Region IV that could be visualized for all MSFrs.

PT-11:

Both Region I and Region II were present for all MSFrs. The presence of fluorophoric region related to tryptophan-like aromatic proteins was more pronounced for higher MSFrs as 450 kDa and 220 kDa. Region III was slightly present in lower MSFrs, i.e., 10 kDa and 3 kDa, whereas Region V could not be visualized indicating that humic-like fluorophoric region was not detected. Region IV was slightly evident for 3 kDa MSFr.

PT-41:

Region I was slightly apparent for all MSFrs along with Region II which exhibited comparatively higher inten-

Table 1 Regional speciation of the EEM fluorescence spectral features of RfOM upon use of the PANI, TiO_2, and PANI-TiO_2 specimens

Specimen	Molecular size fractions					
PANI	450 kDa	220 kDa	100 kDa	30 kDa	10 kDa	3 kDa
Region I	+	+	+	+	+	+
Region II	+ + +	+ + +	+ + +	+ + +	+ +	+ +
Region III	+ + + + +	+ + + +	+ + + +	+ + + +	+ + + + + +	+ + + + + +
Region IV	n.o	n.o	n.o	n.o	+	+
Region V	+	+	+	+ +	+ + +	+ + + +
TiO_2	450 kDa	220 kDa	100 kDa	30 kDa	10 kDa	3 kDa
Region I	+ + +	+ +	+ +	+	+ + +	+ + +
Region II	+ + + + +	+ + +	+ + + + +	+ + + + +	+ + + + +	+ + + + +
Region III	+ + + + + +	+ + + + + +	+ + + + + +	+ + + + + +	+ + + + + +	+ + + + + +
Region IV	+	n.o	+	+	+	+
Region V	+ + +	+ + +	+ + +	+ + + +	+ + + + + +	+ + + + + +
PT-11	450 kDa	220 kDa	100 kDa	30 kDa	10 kDa	3 kDa
Region I	+ +	+ +	+ +	+ +	+ + +	+ +
Region II	+ + + +	+ + + +	+ + +	+ + +	+ + +	+ + +
Region III	n.o	n.o	n.o	n.o	+	+
Region IV	n.o	n.o	n.o	n.o	n.o	+
Region V	n.o	n.o	n.o	n.o	n.o	n.o
PT-41	450 kDa	220 kDa	100 kDa	30 kDa	10 kDa	3 kDa
Region I	+ +	+	+	+	+	+
Region II	+ +	+ +	+ +	+ +	+ +	+ + +
Region III	+	+	+	+	+	+
Region IV	n.o	n.o	n.o	n.o	n.o	+
Region V	n.o	n.o	n.o	n.o	n.o	n.o
PT-81	450 kDa	220 kDa	100 kDa	30 kDa	10 kDa	3 kDa
Region I	+	+	+	+	+	+
Region II	+ +	+ +	+ +	+ +	+ +	+ + +
Region III	+	+	+ +	+ +	+ +	+ +
Region IV	n.o	n.o	n.o	n.o	n.o	+
Region V	n.o	n.o	n.o	n.o	n.o	n.o
PT-14	450 kDa	220 kDa	100 kDa	30 kDa	10 kDa	3 kDa
Region I	+ + +	+ + +	+ +	+ +	+ +	+ +
Region II	+ + + +	+ + +	+ + + +	+ + + +	+ + + +	+ + + +
Region III	+ + + + +	+ + + + +	+ + + + +	+ + + + +	+ + + +	+ + + +
Region IV	n.o	n.o	n.o	n.o	n.o	+
Region V	+ +	+ +	+ +	+ +	+ +	+ +
PT-18	450 kDa	220 kDa	100 kDa	30 kDa	10 kDa	3 kDa
Region I	+	+	+	+	+	+ + +
Region II	+ + + +	+ +	+ + +	+ + +	+ + +	+ + +
Region III	+ + +	+ + +	+ + +	+ + +	+ + +	+ + +
Region IV	n.o	n.o	n.o	n.o	+	+
Region V	+ +	+ +	+ +	+ + +	+ + +	+ + +

n.o. not observed

sity for 3 kDa MSFr. Fulvic-like fluorophores of Region III were also slightly present contrary to lack of Regions IV and V. Lowest MSDr as 3 kDa expressed all regions except minor presence of Region V.

PT-14:

Regions I and II representing aromatic proteins were clearly present for all MSFrs. The presence of Region III was more pronounced in comparison to Region V indicating the foremost occurrence of fulvic-like components with respect to humic-like fluorophoric groups. All MSFrs were entirely lacking Region IV.

PT-18:

The presence of Region II indicating the existence of tryptophan-like aromatic proteins was more pronounced in comparison to tyrosine-like aromatic proteins for all MSFrs. Moreover, 3 kDa MSFr expressed more significant amount of tryrosine-like aromatic proteins whereas 450 kDa MSFr primarily expressed the presence tryptophane-like aromatic proteins. Fulvic-like fluorophores were more evident in lower MSFrs < 30 kDa.

From a general perspective, RfOM was devoid of any Regions as I, II, and IV and mainly composed of Region III and Region V representing fulvic-like and humic-like fluorophoric centers, respectively (Sen-Kavurmaci and Bekbolet 2014). Upon photocatalysis, the presence of Region I and Region II could be associated with an oxidation mechanism prevailing through peptide linkages. The most significant formation was observed upon use of TiO_2 followed by TiO_2 enriched TiO_2-PANI composites as PT-14 and PT-18 whereas PT-11 also expressed a similar pathway resulting in a slight formation tendency in lower MSFrs as < 10 kDa.

Although formation of lower MSFrs was expected via TiO_2 photocatalysis, presence of in situ formed MSFRs of 450 kDa and 220 kDa still expressed all Regions except Region IV. The minor presence of Region IV designated the existence of biomolecules as microbial by-products that could be related to the formation of quinone-quinoid structures which is more pronounced upon TiO_2 photocatalysis. It should also be noted that upon Cu-doped TiO_2 and Fe-doped TiO_2 photocatalysis, mainly fulvic-like and humic-like fluorophoric regions of RfOM were evidently observed in contrary to the other Regions I, II, and IV (Birben et al. 2017; Turkten et al. 2019). The role of PANI could well be elucidated by the respective ratio in PANI-TiO_2 composites. Increasing PANI content resulted in the persistent presence of all Regions along in accordance with the degradation kinetics (Uyguner-Demirel et al. 2023).

Conclusion

This study was conducted to further investigate the complex and competitive reactions between humic molecular size fractions, TiO_2, and PANI under photocatalytic conditions with specific interest on the type of photocatalyst used. It could also be considered as a complementary part of the previously published findings related to (i) preparation and characterization of PANI-TiO_2 composites and (ii) photocatalytic activity assessment of the prepared composites by using RfOM as a model of complex organic matter.

Different tendencies of the diverse MSFr of RfOM towards oxidation were assessed by UV–vis and fluorescence spectroscopic parameters in relation to previous studies on the photocatalytic degradation of RfOM by using TiO_2 and PANI-TiO_2 composites. As confirmed by the investigated parameters, formation of 450 kDa and 220 kDa MSFrs was evident under all conditions indicating in situ formation of higher MSFrs via photocatalysis. Omni presence of 3 kDa MSFr signified the recalcitrant characteristics of the lower molecular size fraction. The dual role of PANI mainly acting as a sensitizer and extending the utilization of visible light in PANI-TiO_2 composites was proven to be highly effective on molecular size distribution of humic matter.

Absorbance-based removal efficiencies under initial and post-photocatalytic conditions indicated a re-formation trend during photocatalysis in the presence of PANI and TiO_2, where higher MSFrs were transformed to lower MSFrs that was notable for < 3 kDa fraction. A_{254}/A_{365} quotient and $SUVA_{280}$ parameter could not be correlated in the presence of PANI-TiO_2 composites in comparison to sole TiO_2 and sole PANI. The effect of increasing PANI content in the composites resulted in removal of all UV–vis parameters (~ 60–70%) of MSFrs in an almost similar trend from 450- to 10-kDa fractions. Moreover, synchronous scan fluorescence profiles of all MSFrs indicated a hypsochromic shift irrespective of the photocatalyst specimen. A detailed 3D presentation of fluorescence as EEM contour plots revealed sample-specific variations being more pronounced in terms of the emergence of tyrosine- and tryptophan-like aromatic proteins. EEM contour plots emphasized the ratio dependency role of PANI on modification of TiO_2.

PANI-TiO_2 composite was proven as an efficient photocatalyst even for the degradation of RfOM acting as a competitor to PANI as well as expressing refractory properties. The study evaluated the applicability of selected spectroscopic parameters as surrogates to determine the characteristics of MSFrs of RfOM upon solar photocatalysis. The presented results suggested index applications for rapid and appropriate assessment of RFOM MSFrs. Completion of UV–vis spectrophotometric analyses with an assessment of fluorescence capacities of RFOM can provide broader information on the changes of their structure. This could be relevant for quality and safety of water resources into which humic matter are occasionally discharged unless being removed during treatment processes.

Supplementary Information The online version contains supplementary material available at https://doi.org/10.1007/s11356-024-34992-2.

Acknowledgements The authors are grateful to the valuable contribution of Prof Y. Karatas, Kırşehir Ahi Evran University, for the preparation of the composite materials.

Author contribution Conceptualization: Miray Bekbolet and Ceyda S. Uyguner-Demirel.

Methodology and experiments: Nazli Turkten.

Writing and original draft preparation: Miray Bekbolet and Ceyda S. Uyguner-Demirel.

Writing—review and editing: Miray Bekbolet and Ceyda S. Uyguner-Demirel.

Supervision: Miray Bekbolet and Ceyda S. Uyguner-Demirel.

Project administration: Ceyda S. Uyguner-Demirel and Miray Bekbolet.

All authors have contributed, read, and approved the final version of the manuscript.

Data availability Data will be made available on reasonable request.

Declarations

Consent to participate Not applicable.

Consent for publication Not applicable.

Competing interests The authors declare no competing interests.

References

Aguiar LG, Siqueira AF (2022) Modeling of catalyst deactivation in humic acid degradation. Ind Eng Chem Res 61(25):8708–8713. https://doi.org/10.1021/acs.iecr.2c00837

Baigorri R, Fuentes M, Gonzalez-Gaitano G, García-Mina JM (2007a) Simultaneous presence of diverse molecular patterns in humic substances in solution. J Phys Chem B 111(35):10577–10582. https://doi.org/10.1021/jp0738154

Baigorri R, Fuentes M, González-Gaitano G, García-Mina JM (2007b) Analysis of molecular aggregation in humic substances in solution. Colloids Surf A: Physicochem Eng Asp 302(1–3):301–306. https://doi.org/10.1016/j.colsurfa.2007.02.048

Bekbolet M, Kavurmaci SS (2015) The effect of photocatalytic oxidation on molecular size distribution profiles of humic acid. Photochem Photobiol Sci 14:576–582. https://doi.org/10.1039/c4pp00262h

Birben NC, Uyguner-Demirel CS, Kavurmaci SS, Gurkan YY, Turkten N, Cinar Z, Bekbolet M (2017) Application of Fe-doped TiO_2 specimens for the solar photocatalytic degradation of humic acid. Catal Today 281(1):78–84. https://doi.org/10.1016/j.cattod.2016.06.020

Chen W, Yu H-Q (2021) Advances in the characterization and monitoring of natural organic matter using spectroscopic approaches. Water Res 190:116759. https://doi.org/10.1016/j.watres.2020.116759

Chen W, Westerhoff P, Leenheer JA, Booksh K (2003) Fluorescence excitation-emission matrix regional integration to quantify spectra for dissolved organic matter. Environ Sci Technol 37:5701–5710. https://doi.org/10.1021/es034354c

Constantino DS, Dias MM, Silva AM, Faria JL, Silva CG (2022) Intensification strategies for improving the performance of photocatalytic processes: a review. J Clean Prod 340:130800. https://doi.org/10.1016/j.jclepro.2022.130800

Dahlén J, Bertilsson S, Pettersson C (1996) Effects of UV-A irradiation on dissolved organic matter in humic surface waters. Environ Int 22(5):501–506. https://doi.org/10.1016/0160-4120(96)00038-4

Dalrymple RM, Carfagno AK, Sharpless CM (2010) Correlations between dissolved organic matter optical properties and quantum yields of singlet oxygen and hydrogen peroxide. Environ Sci Technol 44(15):5824–5829. https://doi.org/10.1021/es101005u

De Haan H, De Boer T (1987) Applicability of light absorbance and fluorescence as measures of concentration and molecular size of dissolved organic carbon in humic Lake Tjeukemeer. Wat Res 21(6):731–734. https://doi.org/10.1016/0043-1354(87)90086-8

Ekande OS, Kumar M (2021) Review on polyaniline as reductive photocatalyst for the construction of the visible light active heterojunction for the generation of reactive oxygen species. J Environ Chem Eng 9(4):105725. https://doi.org/10.1016/j.jece.2021.105725

Etacheri V, Di Valentin C, Schneider J, Bahnemann D, Pillai SC (2015) Visible-light activation of TiO_2 photocatalysts: advances in theory and experiments. J Photochem Photobiol C: Photochem Rev 25:1–29. https://doi.org/10.1016/j.jphotochemrev.2015.08.003

Feng H, Liang YN, Hu X (2022) Natural organic matter (NOM), an underexplored resource for environmental conservation and remediation. Mater Today Sustain 19:100159. https://doi.org/10.1016/j.mtsust.2022.100159

Goh JMS, Wang F, Yeap SP (2022) Surface modification of recycled fabric materials with conductive polyaniline and its role in organic matter adsorption. Int J Environ Sci Technol 19:8945–8956. https://doi.org/10.1007/s13762-021-03757-6

Hatchard CG, Parker CA (1956) A new sensitive chemical actinometer-II. Potassium ferrioxalate as a standard chemical actinometer. Proc R Soc Lond A 235(1203):518–536. https://doi.org/10.1098/rspa.1956.0102

Ilina SM, Drozdova OY, Lapitskiy SA, Alekhin YV, Demin VV, Zavgorodnyaya YA, Shirokova LS, Viers J, Pokrovsky OS (2014) Size fractionation and optical properties of dissolved organic matter in the continuum soil solution-bog-river and terminal lake of a boreal watershed. Org Geochem 66:14–24. https://doi.org/10.1016/j.orggeochem.2013.10.008

Jiang D, Otitoju TA, Ouyang Y, Shoparwe NF, Wang S, Zhang A, Li S (2021) A review on metal ions modified TiO_2 for photocatalytic degradation of organic pollutants. Catalysts 11(9):1039. https://doi.org/10.3390/catal11091039

Korshin GV, Li C-W, Benjamin MM (1997) Monitoring the properties of natural organic matter though UV spectroscopy: a consistent theory. Water Res 31:1787–1795. https://doi.org/10.1016/S0043-1354(97)00006-7

Li Q, Sun L, Zhang Y, Qian Y, Zhai J (2011) Characteristics of equilibrium, kinetics studies for adsorption of Hg(II) and Cr(VI) by polyaniline/humic acid composite. Desalination 266:188–194. https://doi.org/10.1016/j.desal.2010.08.025

Li S, Wang S, Yan B, Yue T (2021) Surface properties of nanoparticles dictate their toxicity by regulating adsorption of humic acid molecules. ACS Sustain Chem Eng 9(41):13705–13716. https://doi.org/10.1021/acssuschemeng.1c02795

Li D, Lin H, Guo L (2023a) Comparisons in molecular weight distributions and size-dependent optical properties among model and reference natural dissolved organic matter. Environ Sci Pollut Res Int 30(20):57638–57652. https://doi.org/10.1007/s11356-023-26398-3

Li X, Wei H, Song T, Lu H, Wang X (2023b) A review of the photocatalytic degradation of organic pollutants in water by modified TiO_2. Water Sci Technol 88(6):1495–1507. https://doi.org/10.2166/wst.2023.288

Lipczynska-Kochany E (2018) Humic substances, their microbial interactions and effects on biological transformations of organic pollutants in water and soil: a review. Chemosphere 202:420–437. https://doi.org/10.1016/j.chemosphere.2018.03.104

Lou T, Xie H (2006) Photochemical alteration of the molecular weight of dissolved organic matter. Chemosphere 65(11):2333–2342. https://doi.org/10.1016/j.chemosphere.2006.05.001

Matthews BJH, Jones AC, Theodorou NK, Tudhope AW (1996) Excitation-emission-matrix fluorescence spectroscopy applied to humic acid bands in coral reefs. Mar Chem 55(3–4):317–332. https://doi.org/10.1016/S0304-4203(96)00039-4

Miano TM, Martin JP, Sposito G (1988) Fluorescence spectroscopy of humic substances. Soil Sci Soc Am J 52(4):1016–1019. https://doi.org/10.2136/sssaj1988.03615995005200040021x

Michalska J, Turek-Szytow J, Dudło A, Kowalska K, Surmacz-Górska J (2023) Evaluation of the applicability of selected analytical techniques for determining the characteristics of humic substances sourced from by-products of the wastewater treatment process. Sci Total Environ 888:164237. https://doi.org/10.1016/j.scitotenv.2023.164237

Ni J, Pignatello JJ (2018) Charge-assisted hydrogen bonding as a cohesive force in soil organic matter: water solubility enhancement by addition of simple carboxylic acids. Environ Sci Process Impacts 20(9):225–1233. https://doi.org/10.1039/C8EM00255J

Petrov D, Tunega D, Gerzabek MH, Oostenbrink C (2017) Molecular dynamics simulations of the standard leonardite humic acid: microscopic analysis of the structure and dynamics. Environ Sci Technol 51(10):5414–5424. https://doi.org/10.1021/acs.est.7b00266

Peuravuori J, Pihlaja K (1997) Molecular size distribution and spectroscopic properties of aquatic humic substances. Anal Chim Acta 337(2):133–149. https://doi.org/10.1016/S0003-2670(96)00412-6

Peuravuori J, Koivikko R, Pihlaja K (2002) Characterization, differentiation and classification of aquatic humic matter separated with different sorbents: synchronous scanning fluorescence spectroscopy. Water Res 36(18):4552–4562. https://doi.org/10.1016/s0043-1354(02)00172-0

Pitois A, Abrahamsen LG, Ivanov PI, Bryan DB (2008) Humic acid sorption onto a quartz sand surface: a kinetic study and insight into fractionation. J Colloid Interface Sci 325:93–100. https://doi.org/10.1016/j.jcis.2008.05.031

Qi B, Aldrich C, Lorenzen L (2004) Effect of ultrasonication on the humic acids extracted from lignocellulose substrate decomposed by anaerobic digestion. J Chem Eng 98(1–2):153–163. https://doi.org/10.1016/j.cej.2003.07.002

Richard C, Coelho C, Guyot G, Shaloiko L, Trubetskoj O, Trubetskaya O (2011) Fluorescence properties of the <5 kDa molecular size fractions of a soil humic acid. Geoderma 163(1–2):24–29. https://doi.org/10.1016/j.geoderma.2011.03.003

Schaumann GE (2006a) Soil organic matter beyond molecular structure Part I: macromolecular and supramolecular characteristics. J Plant Nutr Soil Sci 169(2):145–156. https://doi.org/10.1002/jpln.200521785

Schaumann GE (2006b) Soil organic matter beyond molecular structure Part II: amorphous nature and physical aging. J Plant Nutr Soil Sci 169(2):157–167. https://doi.org/10.1002/jpln.200521791

Scott AI (1964) Interpretation of the ultraviolet spectra of natural products. Pergamon Press, New York

Sen-Kavurmaci S, Bekbolet M (2014) Tracing TiO_2 photocatalytic degradation of humic acid in the presence of clay particles by excitation–emission matrix (EEM) fluorescence spectra. J Photochem Photobiol A: Chem 282:53–61. https://doi.org/10.1016/j.jphotochem.2014.03.011

Shi Y, Zhang C, Liu J, Dai Q, Jiang Y, Xi M, Jia H (2021) Distribution of persistent free radicals in different molecular weight fractions from peat humic acids and their impact in reducing goethite. Sci Total Environ 797:149173. https://doi.org/10.1016/j.scitotenv.2021.149173

Šmejkalová D, Piccolo A (2008) Aggregation and disaggregation of humic supramolecular assemblies by NMR diffusion ordered spectroscopy (DOSY-NMR). Environ Sci Technol 42(3):699–706. https://doi.org/10.1021/es071828p

Thurman EM, Wershaw RL, Malcolm RL, Pinckney DJ (1982) Molecular size of aquatic humic substances. Org Geochem 4(1):27–35. https://doi.org/10.1016/0146-6380(82)90005-5

Trubetskoj OA, Richard C, Voyard G, Marchenkov VV, Trubetskaya OE (2018) Molecular size distribution of fluorophores in aquatic natural organic matter: application of HPSEC with multi-wavelength absorption and fluorescence detection following LPSEC-PAGE fractionation. Environ Sci Technol 52(9):5287–5295. https://doi.org/10.1021/acs.est.7b03924

Turkten N, Bekbolet M (2020) Photocatalytic performance of titanium dioxide and zinc oxide binary system on degradation of humic matter. J Photochem Photobiol A: Chem 401:112748. https://doi.org/10.1016/j.jphotochem.2020.112748

Turkten N, Cinar Z, Tomruk A, Bekbolet M (2019) Copper-doped TiO_2 photocatalysts: application to drinking water by humic matter degradation. Environ Sci Pollut Res Int 26:36096–36106. https://doi.org/10.1007/s11356-019-04474-x

Turkten N, Karatas Y, Bekbolet M (2021) Conducting polymers and photocatalysis: a mini review on selected conducting polymers and photocatalysts as TiO_2 and ZnO. J Photocatal 2:252–270. https://doi.org/10.2174/2665976X02666211201121530

Turkten N, Karatas Y, Uyguner-Demirel CS, Bekbolet M (2023) Preparation of PANI modified TiO_2 and characterization under pre- and post- photocatalytic conditions. Environ Sci Pollut Res Int 30(51):111182–111207. https://doi.org/10.1007/s11356-023-30090-x

Uyguner CS, Bekbolet M (2005a) Implementation of spectroscopic parameters for practical monitoring of natural organic matter. Desalination 176:47–55. https://doi.org/10.1016/j.desal.2004.10.027

Uyguner CS, Bekbolet M (2005b) Evaluation of humic acid photocatalytic degradation by UV-vis and fluorescence spectroscopy. Catal Today 101(3–4):267–274. https://doi.org/10.1016/j.cattod.2005.03.011

Uyguner CS, Bekbolet M, Świetlik J (2007) Chapter 5.1. Natural organic matter: definitions and characterization. In: Nikolau A, Selçuk H, Rizzo L (eds) Control of disinfection by-products in drinking water systems. NOVA Science Publishers Inc., New York-USA, pp 253–277

Uyguner-Demirel CS, Bekbolet M (2011) Significance of analytical parameters for the understanding of natural organic matter in relation to photocatalytic oxidation. Chemosphere 84:1009–1031. https://doi.org/10.1016/j.chemosphere.2011.05.003

Uyguner-Demirel CS, Turkten N, Kaya D, Bekbolet M (2022) Effect of oxidative and non-oxidative conditions on molecular size fractionation of humic acids: TiO_2 and Cu-doped TiO_2 photocatalysis. Environ Sci Pollut Res 29(56):85413–85432. https://doi.org/10.1007/s11356-022-21754-1

Uyguner-Demirel CS, Turkten N, Karatas Y, Bekbolet M (2023) Photocatalytic performance of PANI modified TiO_2: degradation of refractory organic matter. Environ Sci Pollut Res 30:85626–85638. https://doi.org/10.1007/s11356-023-28385-0

Valencia S, Marín JM, Restrepo G, Frimmel FH (2013) Application of excitation–emission fluorescence matrices and UV/Vis absorption to monitoring the photocatalytic degradation of commercial humic acid. Sci Total Environ 442:207–214. https://doi.org/10.1016/j.scitotenv.2012.10.058

Wang J, Ding S, Zheng C, Ma H, Ji Y (2012) Efficient removal of humic acid in aqueous solution using polyaniline adsorbent. Desalin Water Treat 40(1–6):92–99. https://doi.org/10.1080/19443994.2012.671153

Wang J, Ji Y, Ding S, Ma H, Han X (2013) Adsorption and desorption behavior of tannic acid in aqueous solution on polyaniline adsorbent. Chin J Chem Eng 21(6):594–599. https://doi.org/10.1016/S1004-9541(13)60516-9

Wang X, Liang D, Wang Y, Peijnenburg WJ, Monikh FA, Zhao X, Dong Z, Fan W (2022) A critical review on the biological impact of natural organic matter on nanomaterials in the aquatic environment. Carbon Res 1:13. https://doi.org/10.1007/s44246-022-00013-5

Weishaar JL, Aiken GR, Bergamaschi BA, Fram MS, Fujii R, Mopper K (2003) Evaluation of specific ultraviolet absorbance as an indicator of the chemical composition and reactivity of dissolved organic carbon. Environ Sci Technol 37(20):4702–4708. https://doi.org/10.1021/es030360x

Xu H, Guo L (2017) Molecular size-dependent abundance and composition of dissolved organic matter in river, lake and sea waters. Water Res 117:115–126. https://doi.org/10.1016/j.watres.2017.04.006

Yang X, Sun H, Li G, An T, Choi W (2021) Fouling of TiO_2 induced by natural organic matters during photocatalytic water treatment: mechanisms and regeneration strategy. Appl Catal B: Environ 294:120252. https://doi.org/10.1016/j.apcatb.2021.120252

Zhang Y, Li Q, Sun L, Tang R, Zhai J (2010) High efficient removal of mercury from aqueous solution by polyaniline/humic acid nanocomposite. J Hazard Mater 175:404–409. https://doi.org/10.1016/j.jhazmat.2009.10.019

The submission is original, not under consideration for publication elsewhere, and all authors approve the manuscript and agree with its submission to the journal "Environmental Science and Pollution Research." The authors have not submitted the manuscript to a preprint server before submitting it to *Environmental Science and Pollution Research*.